Airfoil Dynamic Stall Performance with Large-Amplitude Motions

M.S. Francis* and J.E. Keesee†
U.S. Air Force Office of Scientific Research, Washington, D.C.

Dynamic lift levels approaching three times the corresponding quasisteady maximum values have been observed to occur and sustain to very high incidence angles (60 deg) when airfoils undergo rapid, large-amplitude pitchup motions at constant rate. Measurements of unsteady surface pressure distributions on two different airfoil shapes have captured the footprint of an energetic separation vortex which originates at the leading edge and exerts a substantial influence on the loading history as it convects downstream. To evaluate the potential of exploiting lifting surface motions as a possible means of load enhancement and control, a dimensionless impulse function that is not dependent on the type of motion is introduced and applied to experimental data. Results suggest that optimum lift performance can be achieved at relatively low pitch rates when the motion is terminated at the rate-determined angle at which the dynamic lift coefficient reaches its maximum value.

Introduction

AIRFOIL dynamic stall is a subject that has received considerable attention in past years, primarily due to its relevance for modeling the aerodynamic effects of torsional helicopter blade oscillations in a high-speed rotor environment.[1-9] The intriguing phenomenology that characterizes the dynamic stall process may, however, be significant in a variety of current and emerging applications which involve dynamic lifting surface motions and where energetic unsteady flow separation can occur. For example, dynamic stall behavior is believed to be the source of unpredicted performance improvements in some wind turbine energy conversion systems. It may also prove to be exceedingly important and even exploitable in the attainment of sustained dynamic maneuvering in the post-stall flight regime.[10-12] It can be important in all applications where the amplitudes of motion are large and where the time constants of the developing flowfield structure and the lifting surface motion are of the same order of magnitude.

The present investigation is concerned with extending the range of airfoil motion conditions beyond the scope of past studies to address situations where relatively low (but unsteady) airfoil pitch rates are accompanied by large amplitude variations in the airfoil pitch angle. The specific focus is on the consequences of the developing dynamically separated flow, emphasizing its influence on airfoil lift and drag generation.

To this end, an experiment has been devised that permits arbitrary airfoil (or wing) pitching motion histories in a low-speed wind tunnel flow environment. Unsteady pressure measurements obtained on the airfoil surfaces have been used to reconstruct phase-averaged surface pressure distributions. These in turn, have been integrated spatially to estimate the force and pitching moment time histories that correlate with the airfoil motion. Two different airfoil shapes were employed in the investigation.

Received May 18, 1984; revision received Jan. 14, 1985. This paper is declared a work of the U.S. Government and therefore is in the public domain.

*Program Manager (present address, Air Force Space Division, Los Angeles, CA). Member AIAA.

†Research Associate, F.J. Seiler Research Laboratory (presently with Headquarters, Strategic Air Command, Offutt AFB, NE).

The Experiment

Motion Generation System

An electromechanical apparatus capable of producing simultaneous motions of an airfoil or wing model in two degrees of freedom has been designed, fabricated, and documented.[13] The concept exploits recent developments in hybrid servo system and microcomputer technologies to provide highly responsive, reproducible motions through a programmable control system. Simultaneous position and velocity feedback have been employed to minimize deviations in cycle-to-cycle motion fidelity.

The system was specifically designed to interface with U.S. Air Force Academy 2×3ft (61×91cm) subsonic wind tunnel. The mechanical drive assembly, including its two dc servomotors, was designed to fit beneath the tunnel test section. A dual scotch-yoke configuration permitted uncoupled model motions in pitch (airfoil geometric angle of attack) and translation in the freestream direction. The model was supported in a vertical position and attached to the drive system by a single hollow steel support shaft that extended upward from the pitch yoke through a slot in the test section floor. This design resulted in minimal aerodynamic interference, but retained a high level of dynamic performance capability.

The two drive motors, each controlling an independent mode of motion, were powered from separate hybrid translator units that, in turn, obtained commands from a single DEC PDP 11/03 microcomputer. The computer control algorithm generated independent, preprogrammed pulse trains that determined the drive motor shaft displacement and rate histories.

A detailed discussion of the complete motion generation apparatus can be found in Ref. 13.

Airfoil Selection and Instrumentation

Two airfoil shapes were employed in the present studies. Initially, a model having a NACA 0012 cross section was fabricated with a rectangular planform of 14 in. (36 cm) span and 6 in (15 cm) chord. The model was constructed from three solid aluminum pieces and excavated to provide interior mounting locations for 19 miniature piezoresistive pressure transducers. Pressure ports were located at the 1, 2.5, 5, 10, 20, 30, 40, 50, 60, 70, 80, and 86.7% chord locations on the suction surface and at the 2, 5, 20, 26.7, 35.3, 60, and 85.3% chord locations on the pressure surface.

Subsequently, a slightly larger NACA 64_1A012(13) profile model with an 8 in. (20 cm) chord and capable of accommodating 20 pressure transducers was fabricated. A similar construction technique provided pressure ports at the leading edge, 2.5, 7, 13, 20, 30, 40, 50, 60, 70, 82.5, and 95% locations on the suction surface and 4, 11.6, 20, 30, 50, 70, 83.4, and 95% chord locations on the pressure surface. This profile has a smaller leading edge radius than the NACA 0012, a parameter believed to be important in the evolution of the dynamic stall flowfield.[2] In addition, the NACA 64_1A012(13) profile possesses a longer favorable pressure gradient region over the surface, a characteristic of modern aircraft wing sections.

The selection of an adequate pressure measurement system was constrained by requirements for high sensitivity, broad frequency response, and relative insensitivity to environmental factors (e.g., temperature and acceleration), coupled with the need for compact physical size. To satisfy these constraints, a scheme involving Endevco model 8507-2 differential pressure transducers embedded within the model interior was employed. Short pieces of flexible vinyl tubing were used to interconnect the heads of each miniature cylindrical transducer to short brass tubes that extended inward from the pressure ports in the model surface. Although this installation method resulted in a somewhat reduced frequency response, the upper roll-off limit of each channel was considered adequate for the present experiments ($f_{max} \geq 1$ kHz).

To provide a stable pressure reference for the transducers, their "reference" tubes were vented to atmospheric pressure in the room exterior to the wind tunnel. This arrangement was judged preferable to alternative schemes using in-tunnel reference sources that might otherwise introduce errors due to unsteady phase lag variations. Steady flow total and static test section pressures were also monitored and employed in the calculation of pressure coefficients.

Neither model was constructed to fully span the wind tunnel test section. Limits on the practical spanwise length were imposed by inertial considerations, which influence realizable model accelerations during unsteady motions. To approximate true airfoil characteristics and maximize flow two-dimensionality, nearly rectangular plexiglass end plates were mounted perpendicular to the span. They extended at least 0.2 chord lengths upstream and downstream of the leading and trailing edges, respectively, and approximately 0.5 chord length above and below the airfoil chord line. They were located equidistant from the pressure tap centerline to give an effective geometric aspect ratio of 1.3 for both airfoil models. This configuration insured that the end plate nearest the wind tunnel floor was located out of the test section wall boundary layer. During initial tests, several measurements of cross-flow velocity near the airfoil surface were made using a hot-wire probe (x-wire configuration) to insure that mean spanwise flow conditions did not exist.

Due to model size and shape limitations, the pitch rotation points of the two airfoils were slightly different. The NACA 0012 model rotated about the 31.7% chord point, while the NACA 64_1A012(13) model rotated at the 37.5% chord location.

Signals from the temperature-compensated miniature pressure transducers were preamplified in close proximity to the model to minimize the voltage drift and noise errors. A DEC PDP 11/45 data acquisition system equipped with 32 analog input channels (DEC Model LPS-11) was employed to process the transducer data and correlate it with the model motion history.

Airfoil Motions: Flow Environment

Although acknowledged to have a potentially profound effect on the dynamic stall process, the "motion time history" is one of the least understood contributors to the overall flow development.[7,8] Several prior studies have been performed in an attempt to assess the significance of this facet of behavior. Besides pure pitching motion, unsteady freestream (or surge) oscillations have been investigated for fixed airfoil incidence conditions.[14,15] Limited studies of combined pitching and surging oscillations have also been conducted.[16,17] Plunging airfoil motion has received recent attention.[18] Despite these efforts, a unified and physically consistent picture of the effects of motion time history has yet to emerge. This is due, in part, to the extremely large range of parametric variables that must be considered to adequately characterize the dynamic effects.

The focus of this study is on the effects of large-amplitude, constant-rate pitching motions as characterized in Fig. 1. The significance of the pitch rate parameter $\dot{\alpha}$ as an influence on the developing flowfield has been discussed previously.[6,19] Unlike the flowfield evolution encountered in previous dynamic stall studies involving harmonic airfoil motions, the onset and development of the leading-edge stall vortex in the present case is not influenced by the decreasing airfoil pitch rate ($\dot{\alpha} \rightarrow 0$) near a relatively low maximum-incidence angle. Instead, the stall process is allowed to develop as the motion continues unaltered well beyond the onset of separation. The occurrence of leading-edge separation and stall vortex development prior to reaching maximum incidence then represents a unique physical situation of special interest.

Following the pitch up from zero incidence, the airfoil was allowed either to remain at the maximum incidence angle (line **a** in Fig. 1) or, in some experiments, returned to the starting condition abruptly (line **b** in Fig. 1). Following the completion of the unsteady motion, a quiescent period ensued to permit the flow to relax to steady flow conditions.

A range of pitch rates over nearly three orders of magnitude was employed in the investigation. Dimensionless pitch rates based on the parameter $k(\equiv \dot{\alpha}c/2U_\infty)$ were in the range of $0.001 \leq k \leq 0.21$. Maximum incidence angles ranged from less than 20 deg to nearly 60 deg for some test cases.

The low end of the rate and amplitude ranges extended from conditions studied by previous investigators to an opposite extreme in which incidence angles well in excess of the induced

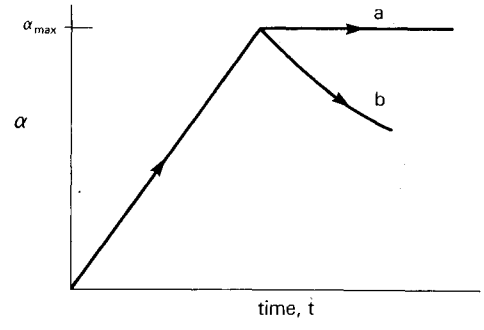

Fig. 1 Constant pitch rate motion waveforms.

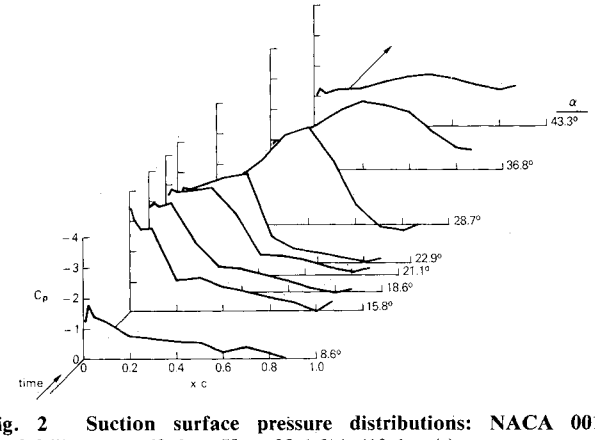

Fig. 2 Suction surface pressure distributions: NACA 0012, $k = 0.047$, $\alpha_{max} = 60$ deg, $U_\infty = 33.1$ ft/s (10.1 m/s).

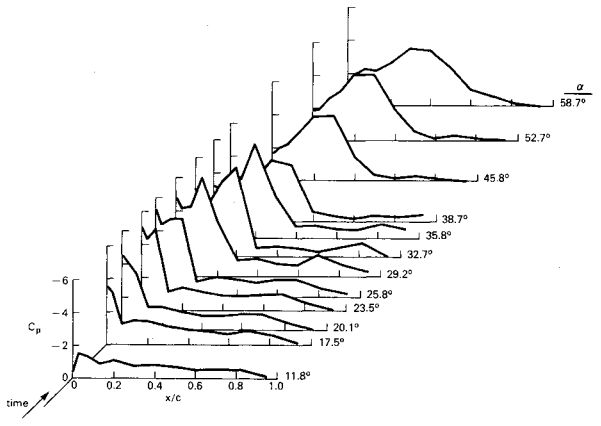

Fig. 3 Suction surface pressure distributions: NACA 64_1A012(13), $k=0.136$, $\alpha_{max}=59$ deg, $U_\infty=32.5$ ft/s (9.9 m/s).

separation condition were achieved for even the highest pitch rates.

Freestream velocity variations from approximately 30 ft/s (9.1 m/s) to nearly 70 ft/s (21.3 m/s) resulted in a reasonable variation of chord Reynolds numbers, $77{,}000 \le Re \le 169{,}000$.

Measurement Techniques and Sources of Error

Since the typical pressure response amplitudes varied over only a small fraction of the rated transducer range (±2 psig), individual "system" calibrations were obtained at regular intervals to minimize calibration errors and to identify defective instrumentation. Except for an early transducer failure (NACA 0012, 95% chord, lower surface measurement location), drift variations did not exceed 3% based on measured maximum levels.

The actual acquisition of data involved repetitive sampling of each of the pressure channels over 25 cycles to obtain a phase-locked ensemble average before proceeding to the next adjacent transducer. This process was repeated around the airfoil until all transducers had provided the requisite output. The pressure time histories were then converted to time-frozen pressure distributions representative of fixed temporal phase points during the motion cycle. Surface pressure data were integrated using an algorithm based on the trapezoidal rule and appropriate coordinate transformations to convert normal and chord forces to lift and drag. This process incorporated local values of the model surface slope, as well as the instantaneous chord line orientation to determine the appropriate transformation angles.

The model motion time history was also stored as part of the data file. Model motion repeatability was assessed both prior to and following each of the experimental cases. Motion variations were not discernible on an oscillograph trace (less than 0.5% variation between the initial and final curves).

No attempt was made to apply wind tunnel corrections to any of the unsteady pressure data. The original choice of relatively small airfoil models was prompted by the desire to minimize errors due to wall effects and blockage.

The possible contamination of observed flow characteristics by disturbances at multiples or subharmonics of the period of motion was a major source of concern. Verification that the convective (closed-circuit) tunnel time constant sufficiently exceeded the period of model motion helped alleviate this concern. Error was further reduced by insuring that neither of these variables was an integer multiple of the other.

No acoustic inteference was detected. It is believed that the energetic character of the induced separation vortices overwhelms any weak excitation provided by experimentally generated acoustic field effects during the significant high-lift portions of the cycle.

The selection of the record size necessary for an accurate representation of the phase-averaged flow behavior was another issue of concern, as was the accompanying cycle deviation from this average. A previous investigation[4] has suggested that a 50 record ensemble is suitable in measurements of similar flow phenomena. Due to the need to minimize electronic and thermal drift and the overall measurement time, it was decided to compromise at a total of 25 records to calculate the phase-averaged pressure history for each transducer. This value was chosen as a result of preliminary tests under several model motion conditions which examined 1, 5, 10, 20, 25, 50, and 100 record averages. Maximum variations from average pressure values did not exceed 10% in the worst case. (This condition was observed for the transducers located near the trailing edge late in the motion cycle when the adjacent flow was characterized by highly turbulent conditions.)

A final factor bearing on the utility of these results is that of the Reynolds number range over which the experiments were conducted. Chord Reynolds numbers and associated boundary-layer development are known to lie within what is considered the "transitional" regime for typical steady flow conditions. However, it is believed that the violent large-amplitude motions employed here readily dominate local shear layer instabilities immediately prior to stall and subsequently when energetic separation vortices are present. A test section turbulence level of approximately 0.15% further precluded the conduct of a quiet experiment and suppressed transitional effects.

Surface Pressure Distributions

The essential features of the dynamic stall flowfield created by harmonic airfoil oscillations in an otherwise steady and uniform freestream have been described by McCroskey and his co-workers.[1-3] The behavior of the flow for what has been termed the "deep-stall" case is of special significance here. For these oscillations in pitch, the flow near the airfoil surface has been observed to remain "attached" during the airfoil upstroke to a point well beyond the static stall incidence angle. This delay in incipient separation is followed by the formation of an energetic vortex structure near the airfoil leading edge, which grows with time and convects downstream over the suction surface as the airfoil motion proceeds. (The visualized evolution of induced separation vortices has recently been documented by several investigators.[20-22]) A strong suction peak in the instantaneous pressure distribution has been observed to remain approximately coincident with the chordwise location of the vortex.

A similar phenomenology is evident in the present experiments. Figures 2 and 3 illustrate the evolution of the suction surface pressure distribution (the "footprint" of the flowfield) for two representative cases. A more complete summary of results covering the broad range of motion conditions studied in this investigation can be found in a companion report.[23] Despite the broad parametric variation of pitch rate and amplitude over the entire set of experiments, the qualitative features were observed to be similar. At incidence angles lower than the static stall value, the shapes of the distributions are suggestive of quasisteady flow (no motion) conditions, except for an apparent lag in the pressure coefficient magnitudes. As the incidence angle increases beyond the static stall value, an "attached flow" distribution persists with suction pressure magnitudes in excess of the equivalent steady flow values.

As the incidence angle continues to increase further, the suction peak is observed to detach from the leading-edge region and move downstream along the suction surface. The imminent detachment condition is evident in the distributions at $\alpha=18.6$ deg in Fig. 2 and noticeable at $\alpha=23.5$ deg in Fig. 3. This behavior is highly suggestive of the dynamic stall vortex observed in previous experiments, since the evolution of the distribution is identical and in the same relative range of incidence angles for comparable pitch rates. In fact, a recent study by Walker et al.[20] provides a visualized record of vortex

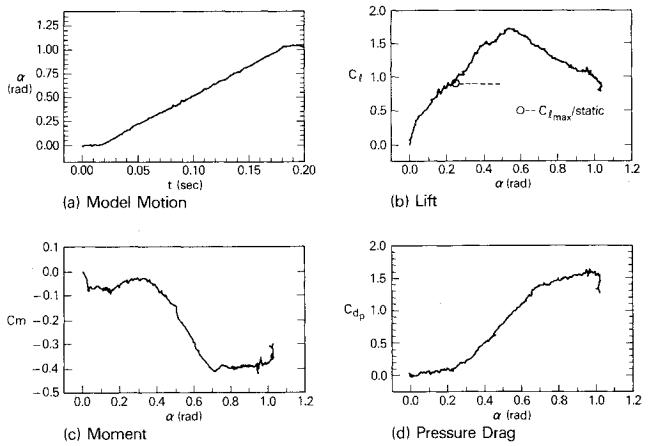

Fig. 4 Force and moment characteristics: NACA 0012, $k=0.047$, $\alpha_{max}=60$ deg, $U_\infty=33.1$ ft/s (10.1 m/s).

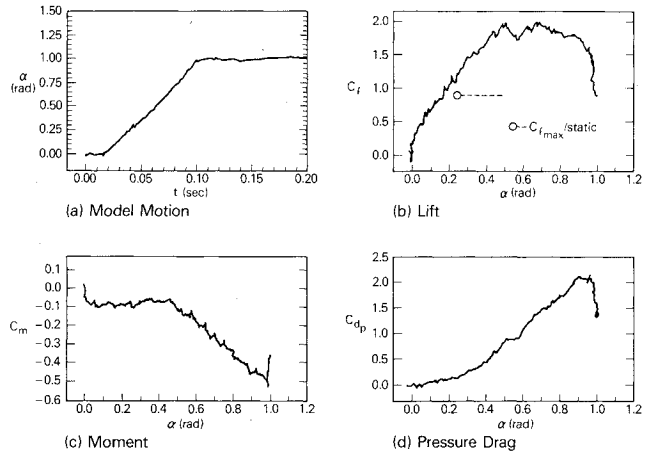

Fig. 5 Force and moment characteristics: NACA 0012, $k=0.089$, $\alpha_{max}=56$ deg, $U_\infty=33.1$ ft/s (10.1 m/s).

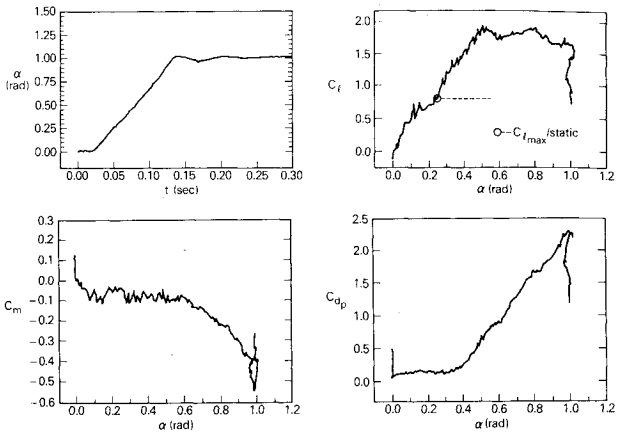

Fig. 6 Force and moment characteristics: NACA 64_1A012(13), $k=0.094$, $\alpha_{max}=59$ deg, $U_\infty=32.1$ ft/s (9.8 m/s).

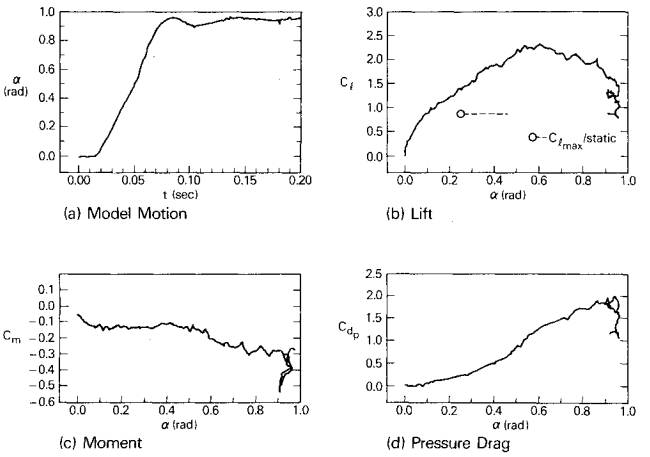

Fig. 7 Force and moment characteristics: NACA 0012, $k=0.130$, $\alpha_{max}=55$ deg, $U_\infty=33.9$ ft/s (10.3 m/s).

evolution under similar flow and motion conditions. As the incidence angle continues to increase even further, the suction peak amplitude continues to grow as it moves toward the trailing edge. The continued growth in local suction magnitude is dependent primarily on the airfoil rotation rate.

At incidence angles well in excess of the static stall value, the pressure peak begins to decrease in magnitude and broaden over the surface as it continues to move rearward. This behavior occurs when the dynamic stall vortex begins to diffuse as it convects into the "wake region" behind the airfoil. As the rotating fluid loses energy, the flowfield structure ultimately relaxes into a separated free shear layer emanating from the airfoil leading-edge region, characteristic of a bluff-body wake. The pressure distributions on both pressure and suction surfaces flatten considerably and approach levels of nearly plus or minus unity, respectively.[23]

The precise nature and timing of these events are closely related to the specific airfoil motion history parameters. It is known that increasing the pitch rate will extend apparent attached flow behavior to higher incidence angles with a concommitant delay in the onset of unsteady leading-edge vortex development.[24,25] All subsequent flow events and their imprint on the surface pressure distribution are similarly delayed.

The maximum incidence angle α_{max} can also influence the flowfield development process. For a given pitch rate and freestream velocity, this parameter determines both the terminal airfoil orientation (boundary conditions) and the point in time when motion-induced unsteady effects cease to be of importance. It is also expected that the initial conditions at the onset of motion play an important role, but that dependence was not addressed in the present investigation.

The shapes of the distributions for both airfoil models are found to exhibit the same general qualitative features. However, for the range of cases considered, the suction peak associated with the NACA 64-series airfoil (Fig. 3) was observed to be steeper and more pronounced in the leading-edge region than that of the NACA 0012 (Fig. 2), especially at high pitch rates. The steep narrow peak also persisted to higher incidence angles on the NACA 64_1A012(13).

Forces and Moments

Unsteady lift, moment, and drag data for both airfoils are displayed with their appropriate motion-time histories in Figs. 4-7 for several representative sets of experimental conditions. Data representing nearly identical motion parameters for the two airfoils are displayed to facilitate a comparison of their aerodynamic performance. The influence of both the pitch rate and amplitude on the character of the force and moment histories is apparent from an examination of these results.

The evolution of the lift coefficient as the motion progresses is significant. The magnitude of the overshoot beyond the static maximum lift value is especially dramatic, as is the persistence of these high lift levels to very large incidence angles. Both results occur irrespective of airfoil shape. In some situations (Figs. 5 and 6), near maximum lift levels were observed to sustain to nearly the maximum incidence condition. It is not clear whether this behavior would have continued to even

higher angles had larger motion amplitudes been employed. Lift values were observed to decrease once the pitchup motion was terminated.

The slopes of the lift curves are also seen to be affected by the extent of the unsteady pitch rate. For reference, steady flow lift data are provided in Fig. 8. At higher values of k, an average lift curve slope steeper than that encountered under quasisteady (no motion) conditions is observed. Therefore, the maximum static lift point is displaced beneath the unsteady lift curves as shown in the figures. Furthermore, the magnitude of this effect is found to increase with higher pitch rate values. This trend appears to be independent of the airfoil shape.

The pressure drag coefficient curves are also found to be profoundly affected by the magnitude of the pitch rate. However, the airfoil shape also appears to play a significant role in the determination of drag. An initial delay in the increase of profile drag with incidence is common under unsteady pitching conditions, but this delay is more pronounced for the NACA 64_1A012(13) airfoil than for the NACA 0012. However, the former airfoil also exhibited a compensating rapid drag rise near the maximum incidence angle, resulting in an overall maximum drag approximately equivalent to that observed with the other shape.

The pitching moment histories displayed in Figs. 4-7 are consistent with the model of a convecting spanwise-oriented vortex dominating the unsteady separated flowfield. An initial lag in pitching moment variation is followed by a pronounced nose-down moment whose amplitude well exceeds the steady flow equivalent. The moment stall of the NACA 0012 airfoil was found to be, in general, less severe than that observed for the 64-series shape. In those cases involving a high pitch rate but with a low value of α_{max}, a severe nose-down moment was observed to occur as the maximum incidence condition was reached.

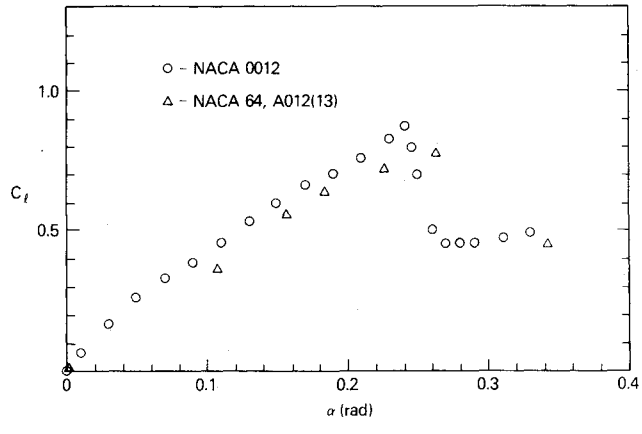

Fig. 8 Steady flow lift characteristics, both airfoils.

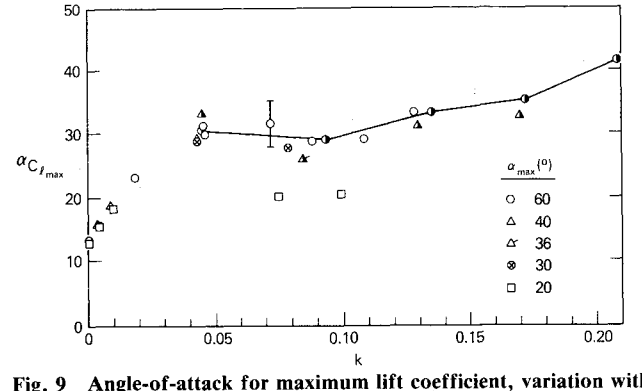

Fig. 9 Angle-of-attack for maximum lift coefficient, variation with pitch rate [open symbols—NACA 0012, half-solid symbols—NACA 64_1A012(13)].

Discussion

The simplest measures of airfoil performance evident from force and moment time histories are a class of variables that can be termed "peak parameters," since they refer to the maximum and/or minimum conditions occurring during the motion cycle. These include, but are certainly not limited to, the angle of attack for which the lift coefficient is a maximum, $\alpha_{C_{\ell max}}$, and the maximum lift coefficient $C_{\ell max}$. A correlation of these variables with limited available flowfield information[20] indicates that this maximum lift condition is coincident with the occurrence of a well-developed separation vortex over the suction surface downstream of and detached from the leading edge.

The variation of $\alpha_{C_{\ell max}}$ as a function of dimensionless pitch rate collectively for the two airfoils is depicted in Fig. 9. Results are provided for several values of the maximum incidence angle. At low pitch rates, the maximum lift angle increases in a nearly linear manner with the pitch rate parameter. At higher values of k and for cases involving large values of α_{max}, this functional relationship changes, as observed from the marked decrease in slope as the dimensionless pitch rate exceeds 0.05. However, the slope continues to remain positive at higher values of k.

A similar parametric dependence can be expected of other variables that earmark specific events in the dynamic stall process. A linear variation in the dynamic stall onset angle with the pitch rate (for low values of the pitch rate) has been measured independently by Daley[24] and Schreck.[25] Harris et al.[26] have suggested that the dynamic stall angle varies with the square root of k based on an empirical extension of Theodoreson's theory. The trend exhibited by the present data is consistent with these results, even if the exact functional dependence is not. This is a reasonable result given that the variable $\alpha_{C_{\ell max}}$ is representative of a nonlinear state of flow development well beyond the initial onset of separation.

At higher pitch rates and for lower values of α_{max}, the angle for maximum lift coefficient and the maximum amplitude of motion appear nearly coincident. This result can be expected in all cases where the motion has been abruptly terminated prior to or in the early stages of stall vortex development.

The above results indirectly suggest that unsteady vortex generation is influenced more profoundly at the lower values of the dimensionless pitch rate. That is, a point of diminishing returns is soon reached if one attempts to delay separation and increase lift by increasing the airfoil pitch rate exclusively.

The maximum lift coefficient $C_{\ell max}$ plotted as a function of the dimensionless pitch rate is depicted for the two airfoils in Fig. 10. The overall shape of the curves is remarkably similar

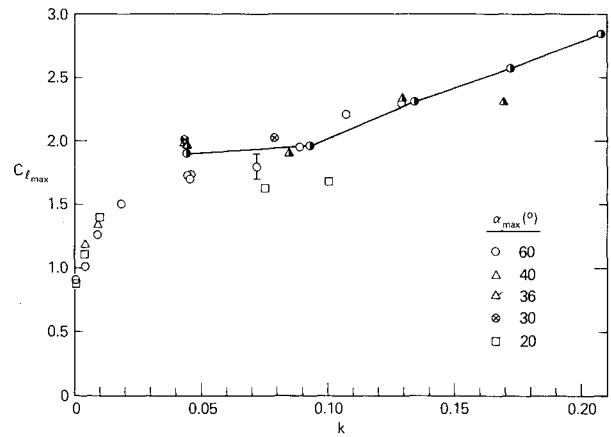

Fig. 10 Maximum lift coefficient variation with pitch rate [open symbols—NACA 0012, half-solid symbols—NACA 64_1A012(13)].

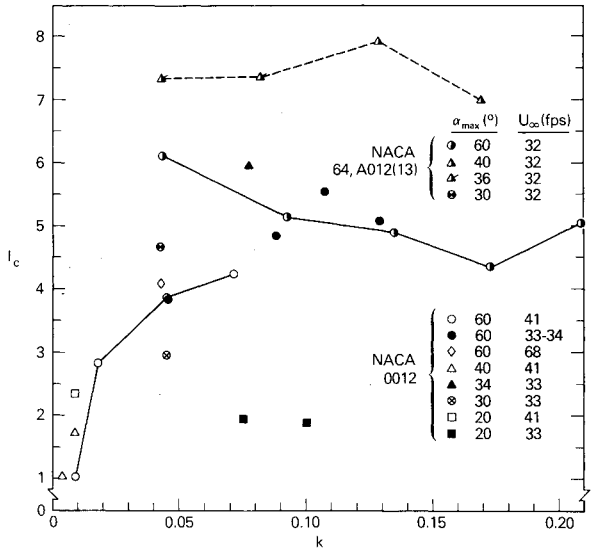

Fig. 11 Dimensionless impulse variation with pitch rate: data survey, both airfoils.

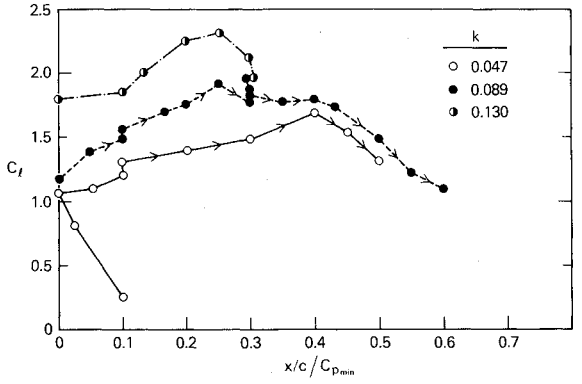

Fig. 12 Lift coefficient variation with suction peak location: NACA 0012, $\alpha_{max} = 60$ deg, $U_\infty = 33$ ft/s (10.1 m/s).

to that found for a corresponding incidence angle variation. The maximum lift coefficient increases rapidly and monotonically at low pitch rates, followed by a decrease in the rate of rise when $k \geq 0.05$. The magnitude of the maximum lift coefficient is also observed to be dependent on the maximum incidence angle of airfoil motion.

The results depicted for the NACA 64_1A012(13) airfoil in Fig. 10 confirm that the increased value of $C_{\ell_{max}}$ with increased pitch rate is not as large at high values of k as it is for lower values. Finally, it is instructive to compare the results for both airfoils. Despite the limited range of the overlap, striking similarities in the gross airfoil performance as measured by the maximum lift coefficient are apparent.

Although the peak values of the variables provide a gross comparison between the various test cases, they do not fully account for the effects of the model motion-time history on overall airfoil performance. It is useful, therefore, to devise other parameters that might more completely characterize the integral performance effects over the motion cycle. It would also be useful to devise a parametric scheme that would allow for comparison of airfoil performance between cases where the motion time history is fundamentally different.

One possible candidate satisfying these criteria, which is also relevant to the lift optimization objective of this study, is the area bounded by the lift-time curve from above and the static maximum lift value from below. This parameter defines an effective impulse function and may be written nondimensionally as

$$I_c = \int_0^{T^*} \Delta C_\ell \cdot \mathrm{d}\left(\frac{t}{\tau}\right)$$

for all

$$\Delta C_\ell \equiv C_\ell - C_{\ell_{\max_s}} \geq 0$$

where $\tau \equiv c/U_\infty$ and $T^* = TU_\infty/c$ is the total time that the lift coefficient exceeds the maximum static value.

The dimensionless impulse defined in this manner is a versatile measure of performance since it incorporates both lift magnitude and duration and is capable of providing equitable comparisons of highly dissimilar motion time histories since the freestream time scale is accounted for implicitly.

The collective variation of I_c with the dimensionless pitch rate for both airfoils is shown in Fig. 11. Results are depicted for several values of the maximum amplitude of motion. Straight line segments have been used to connect points from like data sets to facilitate interpretation. A rapid increase in the impulse parameter at low pitch rates is followed by a more gradual increase at the higher rates of motion. In one group of cases for the NACA 64-series airfoil, a gradual decrease is actually observed to occur with larger values of k.

Significantly, these results suggest that the maximum performance does not monotonically increase with the maximum incidence of motion. This conclusion must be considered in concert with the dependence on pitch rate discussed earlier. Results suggest that maximum performance is achieved by terminating the unsteady motion and maintaining a maximum incidence angle at or near the rate-determined value of $\alpha_{C_{\ell_{max}}}$. The strongest, most persistent vortex is believed to be produced under these conditions. Of course, very large values of α_{max} (much higher than 45 deg) would be geometrically unfavorable for producing aerodynamic lift.

Note that there are discrepancies between the impulse data for the two airfoil cases. Although peak lift levels are comparable at low and moderate pitch rates, the residence time of the unsteady vortex associated with the 64-series airfoil appears to exceed that for the NACA 0012 under some conditions.

Finally, the influence of the motion and magnitude of the suction peak (and, therefore, of the unsteady vortex) on airfoil lift performance can also be examined by relating the suction peak trajectory to corresponding values of the instantaneous lift coefficient. These results are depicted for several large-amplitude motion cases (NACA 0012 airfoil) in Fig. 12. For the lowest value of k, the maximum lift coefficient is observed to occur when the suction peak resides at a chordwise location of approximately 40%. For the intermediate pitch rate case, the location of the suction peak for maximum lift appears to move forward to nearly the 30% chord point. An unusual behavior where the lift apparently continues to increase (by nearly 12%) while the suction peak remains almost stationary is evident in this latter case. This result, suggestive of a temporarily "trapped vortex" condition, was observed for both airfoils in certain situations. However, this trend was not observed in highest rate case. It is also noted that the primary effect of increasing the pitch rate for any given freestream condition is to cause the location of the separation vortex at maximum lift to move closer to the leading edge.

Summary and Conclusions

Results of this experimental investigation involving airfoils undergoing large-amplitude, dynamic pitch-up motions at a constant pitch rate indicate that the dimensionless pitch rate parameter plays an important role in determining the delay and onset of unsteady separation. It also influences the strength of the separation vortex, as manifest in the signature of the upper surface pressure (suction) distribution and the maximum lift coefficient. In general, an increase in pitch rate is found to further delay separation to a higher incidence

angle, but the magnitude of this effect decreases at progressively larger values of the dimensionless pitch rate.

At incidence angles well in excess of the static stall value, the appearance of a steep suction spike on the airfoil upper surface was followed by its subsequent reduction in intensity and spatial diffusion as it traversed downstream. This phenomenological behavior, apparent to varying degrees in all of the experiments, is consistent with that observed by other investigators. The evolution of this peak is believed to be controlled by the behavior of the unsteady leading-edge separation vortex.

Maximum lift coefficients nearly three times the steady flow (no motion) value were observed in some cases at very high pitch rates.

A dimensionless lift impulse function was defined as a suitable measure for comparing the effectiveness of various motion types on sustained lift optimization.

It was observed that neither the highest motion rates nor the largest pitch amplitudes resulted in the maximum values of the pitch impulse parameter. For airfoil rotation at constant rate, the maximization of the integrated unsteady lift appears to occur at intermediate values of the pitch rate, when the incidence angle at which the motion is terminated closely approximates the rate-determined angle for maximum dynamic lift.

Acknowledgments

The research described here was sponsored by the Frank J. Seiler Research Laboratory, (Air Force Office of Scientific Research) under Project 2307, Task F1.

References

[1]Carr, L.W., McAlister, K.W., and McCroskey, W.J. "Analysis of the Development of Dynamic Stall Based on Oscillating Airfoil Experiments," NASA TN D-8382, Jan. 1977.

[2]McCroskey, W.J., Carr, L.W., and McAlister, K.W., "Dynamic Stall Experiments on Oscillating Airfoils," *AIAA Journal*, Vol. 14, Jan. 1976, pp. 57-63.

[3]McCroskey, W.J., "Some Current Research in Unsteady Fluid Dynamics—The 1976 Freeman Scholar Lecture," *Journal of Fluids Engineering*, March 1977, pp. 8-39.

[4]McAlister, K.W., Carr, L.W., and McCroskey, W.J., "Dynamic Stall Experiments on the NACA 0012 Airfoil," NASA TP 1100, Jan. 1978.

[5]Ham, Norman D., "Aerodynamic Loading on a Two-Dimensional Airfoil During Dynamic Stall," *AIAA Journal*, Vol. 6, Oct. 1968, pp. 1927-1934.

[6]Ham, N.D. and Garelick, M.S., "Dynamic Stall Considerations in Helicopter Rotors," *Journal of the American Helicopter Society*, Vol. 13, April 1968, pp. 49-55.

[7]McCroskey, W.J., McAlister, K.W., Carr, L.W., Pucci, S.L., Lambert, O., and Indergand, R.F., "Dynamic Stall on Advanced Airfoil Sections," *Journal of the American Helicopter Society*, Vol. 26, July 1981, pp. 40-50.

[8]McCroskey, W.J. and Pucci, S.L., "Viscous-Inviscid Interaction on Oscillating Airfoils in Subsonic Flow," *AIAA Journal*, Vol. 20, Feb. 1982, pp. 167-174.

[9]Ham, N.D., "Some Recent MIT Research on Dynamic Stall," *Journal of Aircraft*, Vol. 9, May 1972, pp. 378-379.

[10]Herbst, W.B., "Supermaneuverability," *Proceedings of the AFOSR–FJSRL–University of Colorado Workshop on Unsteady Separated Flow*, U.S. Air Force Academy, Colorado Springs, Aug. 1983.

[11]Herbst, W.B., "Dynamics of Air Combat," *Journal of Aircraft*, Vol. 20, July 1983, pp. 594-598.

[12]Ransom, S., "Configuration Development of a Research Aircraft with Post-Stall Maneuverability," *Journal of Aircraft*, Vol. 20, July 1983, pp. 599-605.

[13]Francis, M.S., Keesee, J.E., and Retelle, J.P., Jr., "A Two-Degree-of-Freedom Oscillator for Unsteady Aerodynamics Applications," F.J. Seiler Research Laboratory, AFOSR, Rept. FJSRL-TR-81-0007, ADA-102356, July 1981.

[14]Saxena, L.S., Fejer, A.A., and Morkovin, M.V., "Effects of Periodic Changes in Free Stream Velocity on Flows Over Airfoils Near Static Stall," *Nonsteady Fluid Dynamics, Proceedings of the Winter Annual Meeting ASME*, Dec. 1978, pp. 111-116.

[15]Retelle, J.P., "Unsteady Boundary Layer Flow Reversal in a Longitudinal Oscillating Flow," Frank J. Seiler Laboratory, AFOSR, Tech. Rept. SRL-TR-78-0006, Aug. 1978.

[16]Hsieh, B.J., "Dynamic Stall on Oscillating Airfoils in Oscillating Free Streams," Ph.D. Dissertation, Illinois Institute of Technology, Chicago, May 1979.

[17]Favier, D., Maresca, O., and Rebont, J., "Dynamic Stall Due to Fluctuations of Velocity and Incidence," *AIAA Journal*, Vol. 20, July 1982, pp. 865-871.

[18]Ho, C.M. and Chen, S.H., "Unsteady Wake of a Plunging Airfoil," AIAA Paper 80-1446, July 1980.

[19]Kawashima, S., Yamasaki, M., and Ando, Y., "Aerodynamic Response for the Airfoil Experiencing Sudden Change in Angle of Attach," *Nihon Koku Gakkai; Transactions of the Japan Society for Aeronautical and Space Sciences*, Vol. 21, Aug. 1978.

[20]Walker, J.M., Helin, H.E., and Strickland, J.H., "An Experimental Investigation of an Airfoil Undergoing Large Amplitude Pitching Motions," AIAA Paper 85-0039, Jan. 1985.

[21]Koga, D.J., Reisenthel, P. and Nagib, H.M., "Control of Separated Flowfields Using Forced Unsteadiness," Illinois Institute of Technology, Chicago, IIT Fluids & Heat Transfer Rept. R84-1, Jan. 1984.

[22]Palmer, M. and Freymuth, P., "Analysis of Vortex Development from Visualization of Accelerating Flow Around an Airfoil Starting from Rest," AIAA Paper 84-1568, June 1984.

[23]Francis, M.S., Keesee, J.E., and Retelle, J.P., Jr., "An Investigation of Airfoil Dynamic Stall with Large Amplitude Motions," F.J. Seiler Research Laboratory, AFOSR, Rept. FJSRL-TR-83-0010, ADA-134730, Oct. 1983.

[24]Daley, Daniel C., "Experimental Investigation of Dynamic Stall," MS Thesis, Air Force Institute of Technology, Rept. AFIT/GAE/AA/82D-6, 1983.

[25]Schreck, S.J., "Continued Experimental Investigation of Dynamic Stall," MS Thesis, Air Force Institute of Technology, Rept. AFIT/GAE/AA/83D-21, 1983.

[26]Harris, F.D., Tarzanin, F.J. Jr., and Fisher, R.K. Jr., "Rotor High Speed Performance, Theory vs. Test," *Journal of the American Helicopter Society*, Vol. 15, No. 3, July 1970, pp. 35-44.